LETTER • **OPEN ACCESS**

Morphology of the ferritin iron core by aberration corrected scanning transmission electron microscopy

To cite this article: Nan Jian *et al* 2016 *Nanotechnology* **27** 46LT02

OPEN ACCESS
IOP Publishing

Letters
Nanotechnology

Nanotechnology **27** (2016) 46LT02 (7pp)
doi:10.1088/0957-4484/27/46/46LT02

Letter

Morphology of the ferritin iron core by aberration corrected scanning transmission electron microscopy

Nan Jian[1], Miriam Dowle[1], Richard D Horniblow[2], Chris Tselepis[2] and Richard E Palmer[1]

[1] Nanoscale Physics Research Laboratory, School of Physics and Astronomy, University of Birmingham, Birmingham B15 2TT, UK
[2] Institute of Cancer and Genomic Sciences, University of Birmingham, Birmingham, B15 2TT, UK

E-mail: R.E.Palmer@bham.ac.uk

Received 23 July 2016, revised 22 August 2016
Accepted for publication 14 September 2016
Published 13 October 2016

Abstract

As the major iron storage protein, ferritin stores and releases iron for maintaining the balance of iron in fauna, flora, and bacteria. We present an investigation of the morphology and iron loading of ferritin (from equine spleen) using aberration-corrected high angle annular dark field scanning transmission electron microscopy. Atom counting method, with size selected Au clusters as mass standards, was employed to determine the number of iron atoms in the nanoparticle core of each ferritin protein. Quantitative analysis shows that the nuclearity of iron atoms in the mineral core varies from a few hundred iron atoms to around 5000 atoms. Moreover, a relationship between the iron loading and iron core morphology is established, in which mineral core nucleates from a single nanoparticle, then grows along the protein shell before finally forming either a solid or hollow core structure.

Online supplementary data available from stacks.iop.org/NANO/27/46LT02/mmedia

Keywords: ferritin, iron core, HAADF-STEM, morphology, atom counting

(Some figures may appear in colour only in the online journal)

1. Introduction

Iron is an essential trace element in living organisms. It is vital to many fundamental cellular processes such as oxygen transport, DNA replication and cell division [1–3]. However, excess iron in the body has a potential toxicity due to its capacity to promote the formation of reactive oxygen species, which can lead to damage of the protein and DNA [4]. As such, all organisms need to regulate the amount of free iron available for fundamental cellular processes whilst avoiding iron-induced toxicity. Ferritin, the major iron storage protein, is central to this regulatory mechanism. It can store iron, in the ferric state, and upon cellular demand is mobilised [5–8]. Thus, ferritin is a protein critical to health. A deficiency of ferritin is associated with many diseases, such as Still's disease, Parkinson's disease, sideroblastic anemia, Friedreich's Ataxia and restless legs syndrome [8–10]. In addition, ferritin also commands a good deal of attention in the area of bio-nanotechnology due to its attractive architectural feature, such as its cage structure, stability, non-toxicity and the ability to mineralise other elements [8, 11–13]. Ferritin demonstrates potential for a number of applications, including drug delivery, magnetic recording, and quantum electronics [14–17].

Thus, a deeper understanding of ferritin is required from the perspective of public health and for the development of bionanotechnology.

X-ray structures of the ferritin shell have been known since the 1980s, and show that ferritin molecules in different mammals have very similar structures [2, 18–20]. The apoferritin shell (iron free form of the ferritin protein) has a hollow symmetrical structure formed by 24 sub-units. There are two types of sub-units, H and L, with different amino acid sequences. Apoferritin has an outer diameter of 12 nm and an 8 nm diameter hollow cavity inside, which is available to store mineralised iron. There are 2-fold, 3-fold and 4-fold symmetry axes in the apoferritin molecule. The hydrophilic channels along the eight 3-fold symmetry axes are normally regarded as the major channels for iton entrance [6–8]. The composition of the mineralised iron core is believed to be similar to ferrihydrite [20, 21], a hydrous ferric oxyhydroxide mineral. As the mineralised iron core varies in size and morphology from one ferritin molecule to the next, x-ray crystallography is not suitable for the characterisation of the ferritin core. Transmission electron microscopy is therefore especially useful in the study of the structure of the ferritin iron core.

Electron microscopic studies of ferritin can be traced right back to the 1950s. In 1954, Farrant first observed the iron-containing mineral core, reporting a 5.5 nm iron core diameter and suggesting that it consisted of 4 sub-units, each 2.7 nm in diameter [22]. Six years later, Muir presented a six-sub-unit structure based on his transmission electron microscope (TEM) observations, in which the six sub-units sit at the corners of an octahedron [23]. In 1965, Haggis reported several additional morphologies [24]. To achieve a higher resolution, in 1973, Massover *et al* employed ultrahigh voltage (1–3 MeV) dark field electron microscopy on the horse spleen ferritin and showed that a single core can contain more than one crystallite with different sizes and shapes [25]. The first dark field scanning transmission electron microscopy study of the ferritin core was conducted in 1979 by Crewe and his group [26]. They observed the lattice spacing of the mineral core directly, which, combined with the electron diffraction studies, lead to the conclusion that the core structure is similar to ferrihydrite. A quantitative study with electron energy loss spectra (EELS) in the STEM of individual cores was presented by Pan *et al* who determined the range of core sizes and led to a proposal of a new iron core morphology based on eight sub-units growing from the eight three-fold symmetry channels in the cavity [27–29].

Here we present a study of ferritin's mineral core using aberration-corrected STEM in the high angle annular dark field (HAADF) mode. Moreover, we employed the atom counting method, with size-selected gold clusters as the mass balances, to determine the number of iron atoms in each iron core. The iron loading of the ferritin molecules varies from a few hundred atoms to about 5000 atoms. A relationship between the core morphology and the iron loading is also observed, suggesting that the ferritin core grows from one small nanoparticle along the protein shell to finally form a full, either solid or hollow, iron-containing mineral core.

2. Experimental methods

The ferritin molecules investigated were sourced from Sigma Aldrich UK and are purified from the equine spleen in saline solution. The integrity and quality of the ferritin utilised in this study was verified using SDS PAGE gel electrophoresis and western blotting using polyclonal antibodies to ferritin (1:10 000 dilution, Abcam, rabbit AB69090) [30]. The iron content of ferritin was estimated using a ferrozine assay, a colourimetric assay which determines total iron concentrations post protein degradation and acid liberation of protein-stored iron [31]. This ferritin solution was drop cast onto one half of a 300 mesh TEM copper grid. The TEM grid is covered with a holey carbon film and then a graphene oxide film (EM Solutions) to maximise the contrast. Size-selected $Au_{923\pm46}$ clusters were deposited on the other half of the grid from a magnetron sputtering, gas condensation cluster beam source and mass filtered by a lateral time-of-flight mass selector [32–34]. The cluster beam current was 30 pA and the deposition time was 150 s. The number of size-selected clusters deposited was $\sim 2.8 \times 10^{10}$. Our 200 kV JEOL JEM2100F field emission gun STEM with a spherical aberration corrector (CEOS) was utilised in HAADF mode to image both the ferritins and size-selected gold clusters. The HAADF detector was operated with an inner angle of 62 mrads and outer angle of 164 mrads. The electron dose for each image was 4×10^4 electrons $Å^{-2}$ at 12 million times magnification. No beam shower was performed on the samples in this research to prevent any damage resolving to the sample.

3. Results and discussion

As the apoferritin shell of the ferritin is formed from low atomic number elements like hydrogen, oxygen and carbon, the contrast is not high enough to see the protein shell in the HAADF STEM images. However confirming the existence of the protein shell was crucial for this project. Both SDS PAGE gel electrophoresis (followed by Coomassie blue staining) and western blotting confirmed the integrity of ferritin employed within this study (online supplementary figure S1, table S1). Coomassie blue staining revealed a single band at ca. 20 kDa, which corresponds to the ferritin sub-units (19 kDa ferritin L-chain and 21 kDa H-chain). The Western blotting revealed a single immunoreactive band, which corresponds to a ferritin light chain (L-chain) at ca. 19 kDa. Based on these analysis, the Ferritin degradation was not evident.

The geometrical sizes of the ferritin cores were measured from the HAADF-STEM images. A histogram of the maximum lengths of a total of 114 mineral cores is shown in figure 1(a). We see a peak at 7.5 nm while no core is significantly longer than 8 nm. This implies that the molecule cavities have an inner diameter no greater than 8 nm, which is consistent with previous reports [2, 7, 18]. Furthermore, the most ferritin iron cores have the relative high maximum length, even though their average iron loadings are just close to the half of the maximum capacity (will be shown below),

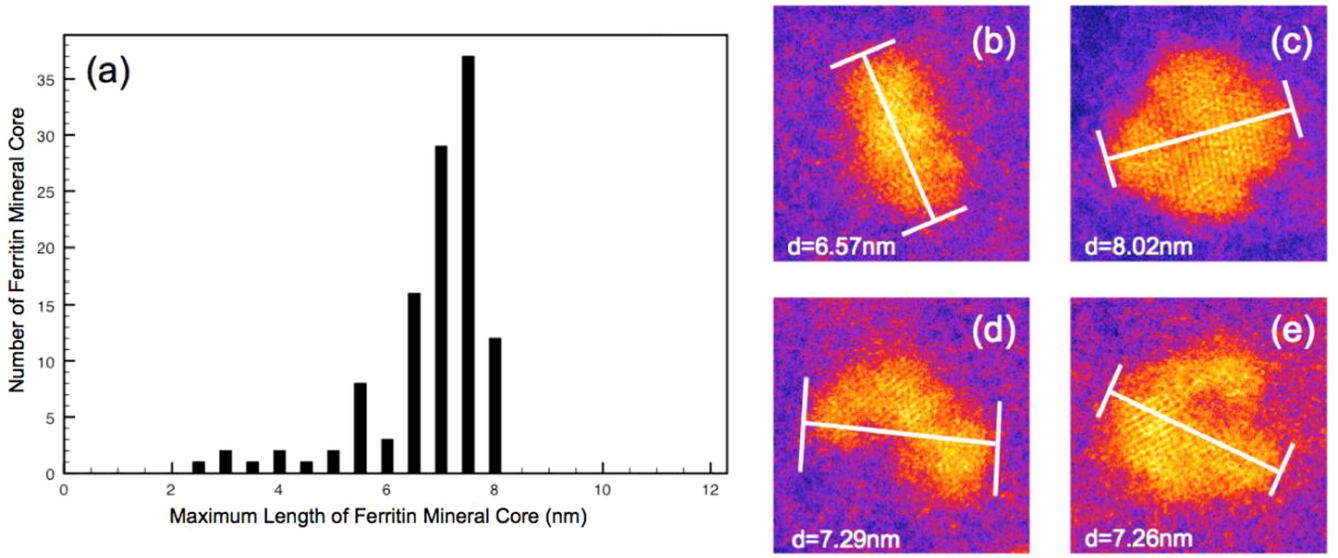

Figure 1. (a) Plot of the maximum length of the ferritin mineral cores. (b)–(e) Examples of HAADF STEM images in which the maximum lengths of the cores are all similar for different core morphologies.

suggesting the iron cores did not grow evenly from small ball to bigger, but grow along the protein shell, so the low loaded ferritin iron cores can also have higher maximum length. As shown in figures 1(b)–(e), the same maximum core length is found independent of the different core morphology. This suggests that all core shapes are limited in size by the protein shell which persists under electron beam irradiation. The lowest maximum length of the iron cores observed is around 2.5 nm, but it does not mean no smaller iron core exists. The Z-contrast property of the HAADF-STEM limited the observation and characterisation of the ultra-small and light elemental cores. The smaller average iron content of the ferritin from chemical analysis comparing with the result from the HAADF-STEM based atom counting also implies that the existence of very small iron cores which did not characterised by the HAADF-STEM.

The number of iron atoms in the ferritin cores, that is, the iron loading, has been obtained by the atom counting method, which compares the integrated HAADF intensity of iron cores to that of size selected $Au_{923\pm46}$ clusters deposited in the same grid, which functions as the mass standards. Background subtraction was carefully performed to include the region adjacent to the mineral core so as to remove the contribution of both the graphene oxide support and the protein shell itself assuming a 3D spherical protein shell of 2 nm thickness. The HAADF intensity contribution by a single proton was obtained through the HAADF intensity of the size selected $Au_{923\pm46}$ cluster divided by the number of protons in each cluster. Then, the number of protons in the ferritin core can be calculated by comparing the integrated HAADF intensities between the ferritin iron core and single proton [35–37]. The error in the iron loading calculation is ±4.36%, based on the mass resolution of size-selected clusters and the measurement error of the STEM intensity. A high resolution image of the iron core crystal structure is shown in figure 2(a), with *d*-spacings of 2.54 Å, 2.51 Å and 2.61 Å and interplanar angles of 61.1°, 59.06° and 60.05°, respectively. These values are consistent with the ferrihydrite crystal structure [38]. Assuming that the mineral cores are indeed ferrihydrite, then the contribution of hydrogen and oxygen atoms can be subtracted, and the actual number of iron atoms in the ferritin cores obtained. The resulting distribution of the iron loading of a total of 103 ferritin molecules is shown in figure 2(b), which shows that the number of iron atoms varies from a few hundred to around 5000. This is a little higher than the maximum iron loading capacity of 4500 iron atoms suggested by many previous researches [2, 7, 29, 39], but there were also studies that reported higher iron loading of about 5000 or higher [10, 40, 41]. This high maximum iron loading can be explained by: first, the 4500 iron capacity is from old experimental measurements, not a theoretical limit, so few hundreds iron atoms fluctuation on the maximum iron loading is acceptable; second, the error of the iron loading calculation also broadened the maximum iron loading about 200 iron atoms, which can also contribute the high maximum iron loading. A chemical analysis of ferritin iron content was also performed, which estimated an average iron content of 2499 ± 9 (SD) iron atoms per ferritin protein by using a ferrozine assay. The Ferrozine calibration curve which made from the standard iron concentrations is shown in figure 5.6. The detail of the estimation is performed in online supplementary figure S2. This value matches well with the average ferritin iron content in the STEM analysis (~2922). The number of atoms estimated by the chemical analysis is slightly smaller, which is because the ferritin with very small iron loading cannot be imaged by the HAADF-STEM method.

As detailed above, different types of morphology are observed in the ferritin cores. We classify them by their 2D projection shape as follows: ‘small circle’, ‘dumbbell’, ‘crescent’, ‘doughnut’ and ‘full raft’. The difference between ‘small circle’ and ‘full raft’ is simply the maximum length,

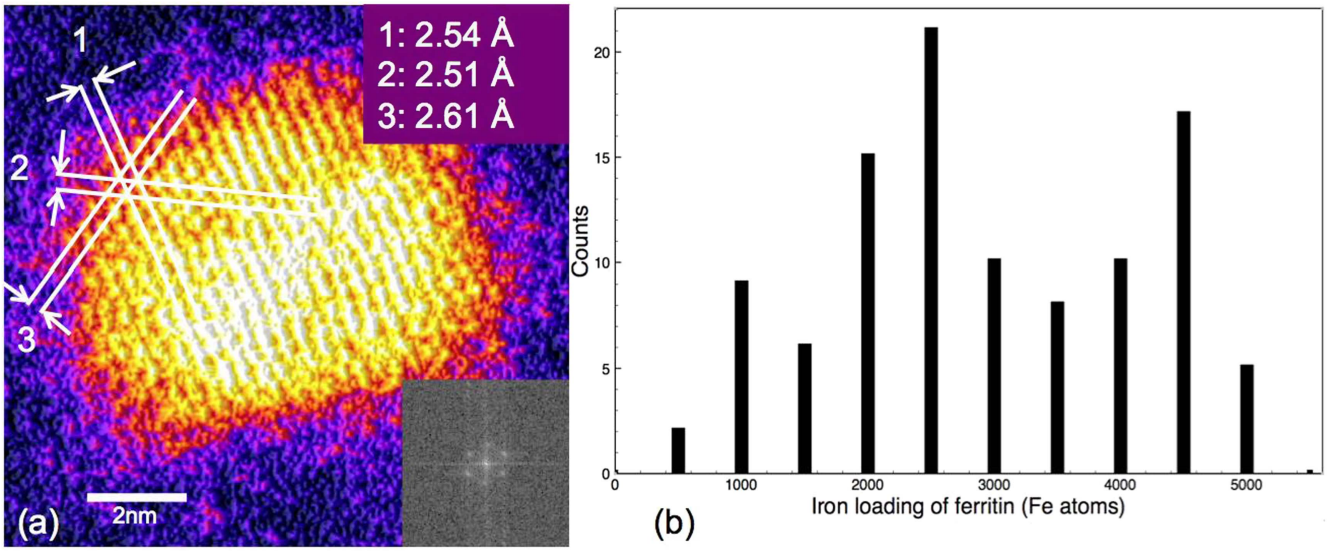

Figure 2. (a) Crystal structure analysis of ferritin iron core. The *d*-spacing and angles labelled are consistent with the ferrihydrite crystal structure. Inset, lower right: the corresponding FFT. (b) Distribution of iron loading in ferritin cores. The number of iron atoms varies from around 500–5000.

with the maximum length of the 'small circle' being lower than 4 nm, e.g. figure 3(a). The 'dumbbell' type is defined as an iron core with aspect ratio larger than 1.5, e.g. figure 3(c). The 'crescent' type cores are the ones that have low intensity at the centre and an imperfect outer shell, e.g. figure 3(e). The 'doughnut' types are the cores that also have low intensity at the centre, but in this case the outer shell is complete, e.g. figure 3(y). The different types of mineral cores are in the different regimes of iron loading. The 'small circle' cores are in the region of a few hundred to around one thousand iron atoms, whereas the 'dumbbell' cores contain from 1000 to 3000 iron atoms, while the 'crescent' cores contain from 1500 to 4000 iron atoms, the 'doughnut' cores contain from 2500 to 5000 iron atoms, and the 'full raft' cores contain from 1500 to 5000 iron atoms. The data indicates that each morphology seems to dominate in a specific regime of iron loading, which should be relevant to understanding the process of the growth of the mineral core. It should be noted that the regimes of different morphology overlap each other somewhat. This is because the STEM images have been classified by their 2D features, which means that in certain regimes of nuclearities, different morphology types can actually reflect the same 3D morphology with different 2D projections. For example, if a disk-like iron core contains around 2500 iron atoms (so the protein shell is half full) and has a hole in its centre, it will be considered as 'doughnut'. However, if it stands vertically on the surface, the image will show a 'dumbbell' type core.

From the analysis of iron loadings and morphologies of the ferritin mineral cores, a morphology 'atlas' was generated and is shown in figure 3. This shows how the morphologies change with iron loadings. The smallest iron loading corresponds to the 'small circle' morphology, then as the iron loading increases, the morphology changes in the following sequence: from 1000 iron atoms, the 'dumbbell' type morphology appears up to 3000 iron atoms, from 1500 iron atoms, the 'crescent' type morphology emerges and persists up to 4000 iron atoms, the 'doughnut' is observed from 2500 to 4500 iron atoms; finally the 'full raft' appears from 1500 to 5000 iron atoms, with the largest iron loading matching the 'full raft' morphology.

The eight channels which correspond to the 3-fold symmetry axes of apoferritin are regarded as the main entrances for iron mineralisation. The dissolved Fe^{2+} ions are oxidised to form Fe^{3+} in the catalytic ferroxidase site, which is located in the centre of the helical bundle of ferritin sub-units and atom mineralisation takes place on the H sub-unit of the protein shell to form the initial mineral core [2, 7, 11, 19]. Previous research suggests that when the mineral core is formed, the surface of the growing core will act as a site for oxidation deposition [2, 42–45], such that deposition on the mineral core is faster than on the inside of the protein shell. This accounts for the well-defined quasi-spherical morphology of the cores at low iron loading. Many of the mineral core structures in figure 3 of higher mass can be rationalised as connected assembles of these 'small circle', formed nucleation at two (figure 3(b)), three (figure 3(e)) or more (figure 3(w)) different sites within the protein cavity. Moreover, the 'crescent' shapes observed, like in figures 3(e) and (q), suggest a tendency for these individual precipitates to nucleate on the inner surface of the protein shell. The observation of a quasi-hollow (almost) full mineral core can be seen as a further manifestation of the preferred nucleation in the inner wall of the protein shell.

In all electron microscopy research, there is the question of how much the electron beam itself affects the sample. In our work, the electron dose is 4×10^4 electrons $Å^{-2}$. Research on the electron beam damage to ferritin [27, 29] used EELS to detect the valence change of Fe in the ferritin iron core. At 200 kV in the TEM, Fe^{3+} began to be reduced to Fe^{2+} when the electron dose was above $\sim 10^5$ electrons $Å^{-2}$,

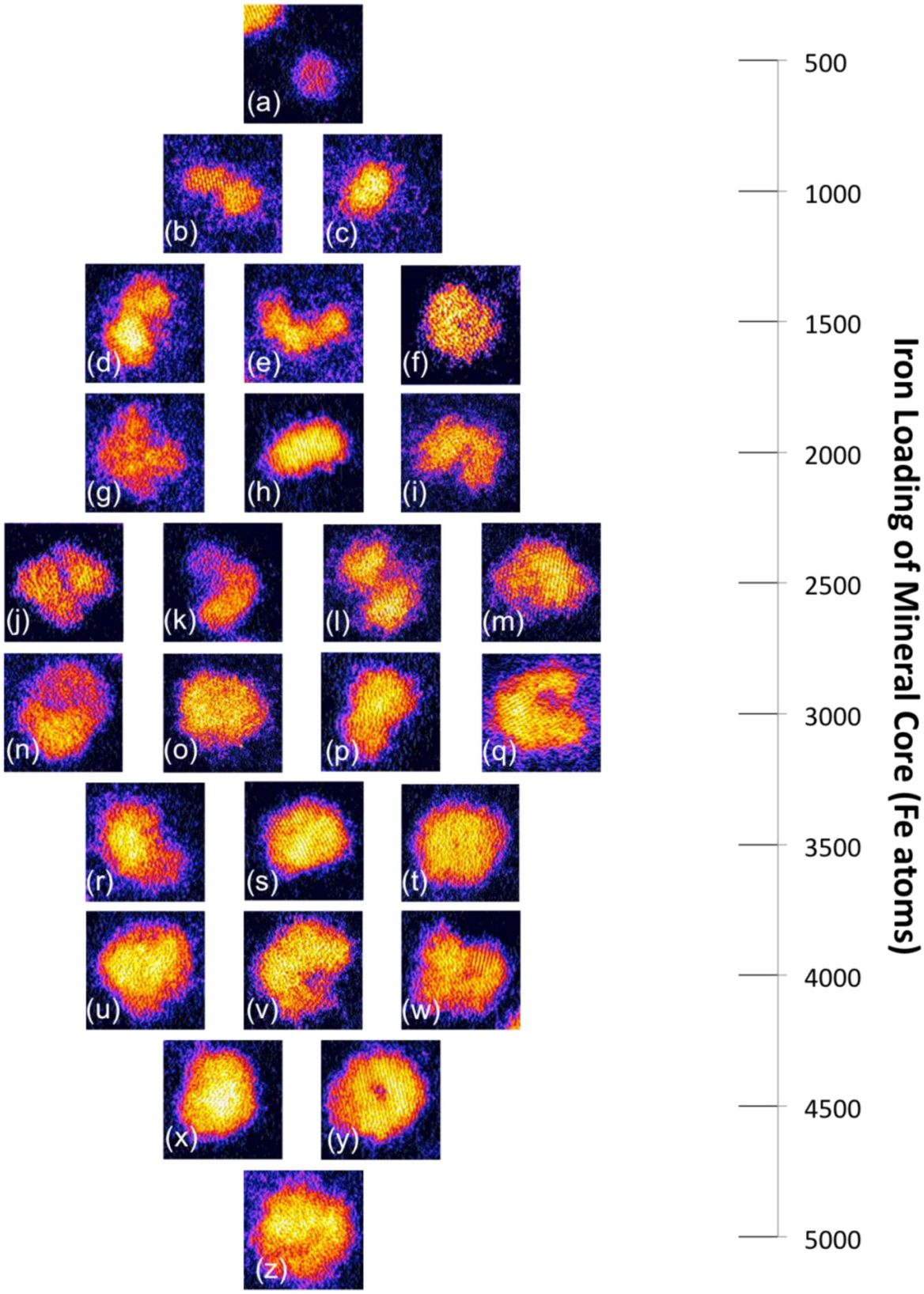

Figure 3. The morphology 'atlas' of the ferritin iron core with different iron loading regions. From (a) to (z) are the representative images for every type of morphology oberserved in dfferent size ranges. For example, there is only one morphologic 'small circle' found in the size range of ~500 iron atoms, as shown in (a), while all four types of morphology, (j) 'doughnut', (k) 'crescent', (l) 'dumbbell' and (m) 'full raft', are observed in the size range ~2500 iron atoms. The frame size of the ferritin example image is 8.24 × 8.24 nm.

so our $\sim 10^4$ electrons $Å^{-2}$ can be seen as a 'safe electron dose'. In a 100 kV STEM study, the electron beam had no influence on the iron valence state at an electron dose of 10^5 electrons $Å^{-2}$, but the percentage of the Fe–O octahedral coordination did decrease from ~75% at 10 electrons $Å^{-2}$ to ~63% at the dose we employed in our research. Overall, it is reasonable to deduce that the electron beam effect is not very significant in our study. Furthermore, the maximum length analysis in figure 1 showed that no ferritin core is larger than the ferritin protein shell inner diameter of 8 nm, which again suggests that the iron core and protein cavity morphology is not changed significantly by the electron beam.

4. Conclusion

The morphology of the ferritin mineral core has been investigated via aberration-corrected HAADF STEM. The iron loading of the ferritin cores has been determined by the atom counting method with size-selected Au clusters as mass balances. The number of iron atoms in the core varies from a few hundred to ~5000 atoms. Analysis of the closest separation distances between the cores and their maximum length has confirmed the preservation of the ferritin protein shell. Different types of morphology of the iron-containing cores were identified and classified as a function of their iron loading. Growth of the mineral core begins with a small circle morphology. Nucleation and growth of further such nanoparticles on the internal surface of the protein shell accounts for the 'dumbbell' and 'crescent' morphologies observed before near complete filling of the cavity with a solid or hollow, quasi-spherical core. The mineralisation process we found will be helpful in a more accurate nanoparticle synthesis in ferritin protein and improve the performance of the ferritin based drug delivery system. The method we used to determine the iron loading of ferritin can be extended to other metal containing proteins and can also be a new medical test method to develop more specific therapies for the ferritin-related diseases.

Acknowledgments

We acknowledge financial support from the EPSRC, the TSB and the University of Birmingham. The cluster beam source and STEM instrument employed in this research was obtained through the Birmingham Science City project 'Creating and Characterising Next Generation Advanced Materials,' supported by Advantage West Midlands (AWM) and funded in part by the European Regional Development Fund (ERDF).

References

[1] Andrews N C and Schmidt P J 2007 Iron homeostasis *Annu. Rev. Physiol.* **69** 69–85
[2] Harrison P M and Arosio P 1996 The ferritins: molecular properties, iron storage function and cellular regulation *Biochim. Biophys. Acta—Bioenerg.* **1275** 161–203
[3] Zhao G, Ceci P, Ilari A, Giangiacomo L, Laue T M, Chiancone E and Chasteen N D 2002 Iron and hydrogen peroxide detoxification properties of DNA-binding protein from starved cells. A ferritin-like DNA-binding protein of Escherichia coli *J. Biol. Chem.* **277** 27689–96
[4] Gutteridge J M C and Halliwell B 1989 1 Iron toxicity and oxygen radicals *Baillieres. Clin. Haematol.* **2** 195–256
[5] Liu X and Theil E C 2005 Ferritins: dynamic management of biological iron and oxygen chemistry *Acc. Chem. Res.* **38** 167–75
[6] Finazzi D and Arosio P 2014 Biology of ferritin in mammals: an update on iron storage, oxidative damage and neurodegeneration *Arch. Toxicol.* **88** 1787–802
[7] Ford G C, Harrison P M, Rice D W, Smith J M, Treffry A, White J L and Yariv J 1984 Ferritin: design and formation of an iron-storage molecule *Phil. Trans. R. Soc.* B **304** 551–65
[8] Theil E C 2013 Ferritin: the protein nanocage and iron biomineral in health and in disease *Inorg. Chem.* **52** 12223–33
[9] Barton J and Bertoli L 1996 Hemochromatosis: the genetic disorder of the twenty-first century *Nat. Med.* **2** 394–5
[10] Quintana C, Bellefqih S, Laval J Y, Guerquin-Kern J L, Wu T D, Avila J, Ferrer I, Arranz R and Patiño C 2006 Study of the localization of iron, ferritin, and hemosiderin in Alzheimer's disease hippocampus by analytical microscopy at the subcellular level *J. Struct. Biol.* **153** 42–54
[11] Jutz G, van Rijn P, Santos Miranda B and Böker A 2015 Ferritin: a versatile building block for bionanotechnology *Chem. Rev.* **115** 1653–701
[12] Huard D J E, Kane K M and Tezcan F A 2013 Re-engineering protein interfaces yields copper-inducible ferritin cage assembly *Nat. Chem. Biol.* **9** 169–76
[13] Theil E C and Turano P 2013 Metalloenzymes: cage redesign explains assembly *Nat. Chem. Biol.* **9** 143–4
[14] Yamashita I 2001 Fabrication of a two-dimensional array of nano-particles using ferritin molecule *Thin Solid Films* **393** 12–8
[15] Jain S K, Chaurasiya A, Gupta Y, Jain A, Dagur P, Joshi B and Katoch V M 2008 Development and characterization of 5-FU bearing ferritin appended solid lipid nanoparticles for tumour targeting *J. Microencapsul.* **25** 289–97
[16] Miura A, Tsukamoto R, Yoshii S, Yamashita I, Uraoka Y and Fuyuki T 2008 Non-volatile flash memory with discrete bionanodot floating gate assembled by protein template *Nanotechnology* **19** 255201
[17] Fujikawa S, Muto E and Kunitake T 2007 Embedding of individual ferritin molecules in large, self-supporting silica nanofilms *Langmuir* **23** 4629–33
[18] Crichton R R and Declercq J P 2010 X-ray structures of ferritins and related proteins *Biochim. Biophys. Acta—Gen. Subj.* **1800** 706–18
[19] Lewin A, Moore G R and Le Brun N E 2005 Formation of protein-coated iron minerals *Dalton Trans.* **22** 3597–610
[20] Cowley J M, Janney D E, Gerkin R C and Buseck P R 2000 The structure of ferritin cores determined by electron nanodiffraction *J. Struct. Biol.* **131** 210–6
[21] Chasteen N D and Harrison P M 1999 Mineralization in ferritin: an efficient means of iron storage *J. Struct. Biol.* **126** 182–94
[22] Farrant J 1954 An electron microscopic study of ferritin *Biochim. Biophys. Acta* **13** 569–76
[23] MUIR A R 1960 The molecular structure of isolated and intracellular ferritin *Q. J. Exp. Physiol. Cogn. Med. Sci.* **45** 192–201
[24] Haggis G H 1965 The iron oxide core of the ferritin molecule *J. Mol. Biol.* **14** 598–602

[25] Massover W H, Lacaze J C and Durrieu L 1973 The ultrastructure of ferritin macromolecules: I. Ultrahigh voltage electron microscopy (1–3 MeV) *J. Ultrastruct. Res.* **43** 460–75
[26] Ohtsuki M, Isaacson M S and Crewe A V 1979 Dark field imaging of biological macromolecules with the scanning transmission electron microscope *Proc. Natl Acad. Sci. USA* **76** 1228–32
[27] Pan Y, Brown A, Brydson R, Warley A, Li A and Powell J 2006 Electron beam damage studies of synthetic 6-line ferrihydrite and ferritin molecule cores within a human liver biopsy *Micron* **37** 403–11
[28] Pan Y-H, Brown A, Sader K, Brydson R, Gass M and Bleloch A 2008 Quantification of absolute iron content in mineral cores of cytosolic ferritin molecules in human liver *Mater. Sci. Technol.* **24** 689–94
[29] Pan Y H, Sader K, Powell J J, Bleloch A, Gass M, Trinick J, Warley A, Li A, Brydson R and Brown A 2009 3D morphology of the human hepatic ferritin mineral core: new evidence for a subunit structure revealed by single particle analysis of HAADF-STEM images *J. Struct. Biol.* **166** 22–31
[30] Horniblow R D, Dowle M, Iqbal T H, Latunde-Dada G O, Palmer R E, Pikramenou Z and Tselepis C 2015 Alginate-iron speciation and its effect on *in vitro* cellular iron metabolism *PLoS One* **10** 1–14
[31] Rebouche C J, Wilcox C L and Widness J A 2004 Microanalysis of non-heme iron in animal tissues *J. Biochem. Biophys. Methods* **58** 239–51
[32] Pratontep S, Carroll S J, Xirouchaki C, Streun M and Palmer R E 2005 Size-selected cluster beam source based on radio frequency magnetron plasma sputtering and gas condensation *Rev. Sci. Instrum.* **76** 045103
[33] Pratontep S, Preece P, Xirouchaki C, Palmer R E, Sanz-Navarro C F, Kenny S D and Smith R 2003 Scaling relations for implantation of size-selected Au, Ag, and Si clusters into graphite *Phys. Rev. Lett.* **90** 055503
[34] von Issendorff B and Palmer R E 1999 A new high transmission infinite range mass selector for cluster and nanoparticle beams *Rev. Sci. Instrum.* **70** 4497
[35] Wang Z W, Toikkanen O, Yin F, Li Z Y, Quinn B M and Palmer R E 2010 Counting the atoms in supported, monolayer-protected gold clusters *J. Am. Chem. Soc.* **132** 2854–5
[36] Jian N, Stapelfeldt C, Hu K, Fröba M and Palmer R 2015 Hybrid atomic structure of the Schmid cluster $Au_{55}(PPh_3)_{12}Cl_6$ resolved by aberration-corrected STEM *Nanoscale* **7** 885–8
[37] Jian N and Palmer R E 2015 Variation of the core atomic structure of thiolated $(Au_xAg_{1-x})312 \pm 55$ nanoclusters with composition from aberration-corrected HAADF STEM *J. Phys. Chem.* C **119** 11114–9
[38] Drits V 1993 Structural model for ferrihydrite *Clay Miner.* **28** 185–207
[39] Rothen A 1944 Ferritin and apoferritin in the ultracentrifuge: studies on the relationship of ferritin and apoferritin; precision measurements of the rates of sedimentation of apoferritin *J. Biol. Chem.* **152** 679–93
[40] Shuman H and Somlyo A P 1982 Energy-filtered transmission electron microscopy of ferritin *Proc. Natl Acad. Sci. USA* **79** 106–7
[41] Crichton R R, Ponce-Ortiz Y, Koch M H, Parfait R and Stuhrmann H B 1978 Isolation and characterization of phytoferritin from pea (*Pisum sativum*) and lentil (*Lens esculenta*) *Biochem. J.* **171** 349–56
[42] Macara I G, Hoy T G and Harrison P M 1973 The formation of ferritin from apoferritin. Catalytic action of apoferritin *Biochem. J.* **135** 343–8
[43] Levi S and Luzzago A 1988 Mechanism of ferritin iron uptake: activity of the H-chain and deletion mapping of the ferro-oxidase site *J. Biol. Chem.* **263** 18086–92
[44] Bauminger E R, Harrison P M, Nowik I and Treffry A 1989 Mössbauer spectroscopic study of the initial stages of iron-core formation in horse spleen apoferritin: evidence for both isolated Fe(III) atoms and oxo-bridged Fe(III) dimers as early intermediates *Biochemistry* **28** 5486–93
[45] López-Castro J D, Delgado J J, Perez-Omil J A, Gálvez N, Cuesta R, Watt R K and Domínguez-Vera J M 2012 A new approach to the ferritin iron core growth: influence of the H/L ratio on the core shape *Dalton Trans.* **41** 1320